

Received September 23, 2019, accepted October 15, 2019, date of publication October 18, 2019, date of current version October 30, 2019.

Digital Object Identifier 10.1109/ACCESS.2019.2948230

A Self-Alignment Method of MEMS Biaxial Rotation Modulation Strapdown Compass for Marine Applications

WEIQUAN HUANG AND MENGHAO LI 

College of Automation, Harbin Engineering University, Harbin 150001, China

Corresponding author: Menghao Li (lmh950605@163.com)

This work was supported in part by the National Natural Science Foundation of China under Grant 61633008, and in part by the National Nature Science Foundation of China under Grant 61773132.

ABSTRACT Self-alignment of strapdown inertial navigation systems incorporating micro-electro-mechanical systems (MSINS) is a great challenge for marine applications. In this paper, a self-alignment method for a rotating MEMS strapdown compass is proposed with the aim of solving this problem. First, based on an analysis of biaxial rotation modulation and initial alignment of the strapdown compass, a self-alignment method is presented and verified. Second, by analyzing the effects of biaxial rotation modulation, the proposed method is improved by speeding up the rotation and reducing the stop time of the biaxial rotation mechanism to shorten the initial alignment time, which effectively suppresses the influence of MEMS noise on the initial alignment error angle. The influence of ship swinging on the initial alignment error angle is also analyzed. The efficiency of the method is verified by experiments on a swinging base. Finally, a parameter adjustment approach is presented that allows the proposed method to be used with different types of MEMS. This approach is validated by experiments. All the experimental results demonstrate the efficiency and precision of the proposed method.

INDEX TERMS Biaxial rotation modulation, MEMS, self-alignment, strapdown compass.


I. INTRODUCTION

An MEMS strapdown inertial navigation system (MSINS) is a combination of a strapdown inertial navigation system (SINS) and micro-electro-mechanical systems (MEMS) technology. Such systems are at the forefront of navigation research and are already in use for moderate to low-precision navigation of ships, owing to their advantages of, among other things, high reliability, low cost, and capability of miniaturization. Obtaining the initial alignment that determines the initial attitude is a prerequisite for navigational computation in a SINS [1]. This initial self-alignment relies on the inertial measurement unit (IMU) itself to complete the initial alignment without the aid of external information.

Normally, the MEMS initial alignment depends on the MEMS accelerometer and magnetometer to determine horizontal attitude and heading attitude [2]. However, this method can determine the attitude only on a static base and in the

absence of magnetic interference. It is not suitable for marine applications, where there are swinging motion and strong magnetic interference [3]. To remove the limitation imposed by the use of a magnetometer, a single-antenna method is adopted in [4]. However, it is only used on a moving base. To allow both swinging and static bases, a double-antenna method is adopted in [5], although this method is not suitable for use in bad weather. In [6], transmission alignment methods are adopted to avoid interference with GPS signals. However, the above methods are not suitable for self-alignment. Compared with the method proposed in this paper, the proposed alignment method is suitable for self-alignment on a swinging base without magnetometers in any weather environments.

Self-alignment methods are widely used in high-precision SINS, with analytic coarse alignment [7] and inertial alignment [8] being the most commonly adopted. Analytic alignment constructs two non-collinear vectors to determine the initial strapdown matrix and to calculate the initial attitude. However, this method can only be used with a gyroscope

The associate editor coordinating the review of this manuscript and approving it for publication was Hassen Ouakad .

whose output is sensitive to the angular velocity of the earth, so it is not suitable for MEMS self-alignment. Inertial alignment first defines the carrier inertial frame, and subsequently, the geo-northward information is obtained by rotating this coordinate frame. In recent years, rotation modulation has attracted increasing attention. In [9], a self-alignment method for MSINS is proposed that combines inertial alignment and the single-axis rotation modulation. However, this method is not suitable for all types of MEMS. Compared with the method proposed in this paper, the proposed alignment method is suitable for MEMS, even any type of MEMS.

Since the gyroscope drift of MEMS is hardly sensitive to the angular velocity of the earth, the initial self-alignment of MSINS has become a matter of some concern. This drift is the main factor influencing MEMS initial self-alignment. Therefore, MEMS biaxial rotation modulation is used to modulate the direct current and slow signals of MEMS IMU drift into sinusoidal and alternating current signals by a periodic rotation. The navigational errors caused by the MEMS IMU can be offset during a complete rotation period to improve the accuracy of MSINS [10], [11]. Because of the characteristic of high precision, the traditional biaxial rotation mechanism is widely used in high-precision SINS. However, due to its high cost production and large volume, the traditional biaxial rotation mechanism is not applicable to MSINS. In the present paper, a biaxial rotation mechanism is developed whose cost of production is lower than that of a traditional biaxial rotation mechanism. Compared with the traditional rotation mechanism, this biaxial rotation mechanism cannot be accurate as the traditional rotation mechanism, but it not only meets the requirements for low-cost MSINS, but also provides the required precision of MSINS.

Biaxial rotation modulation is an error self-compensation technique that is effective for improving navigational accuracy given existing device accuracy. However, biaxial rotation modulation on its own cannot provide MEMS gyroscopes with sufficient sensitivity to the angular velocity of the earth. Therefore, the initial alignment method for high-precision SINS cannot be applied to the initial self-alignment of MSINS. The random noise of MEMS gyroscopes can be suppressed effectively by a number of methods, such as wavelet denoising [12] and moving average filters [13]. However, the use of these methods does not significantly improve the accuracy of navigation, because navigational computations involve low-pass characteristics. Thus, it is necessary to adopt a higher order low-pass filter to complete the initial self-alignment of MSINS.

In this paper, a novel self-alignment method of MSINS on a swinging base is proposed that not only completes the initial alignment of MSINS in an autonomous manner at medium and low precision, but also does so with the required accuracy. The proposed self-alignment method is an improvement of the strapdown compass alignment method, combined with biaxial rotation modulation. Its feasibility is verified by experiments. The errors in the horizontal and heading attitudes are found to be 0.2° and 1.5° , respectively [14].

A frequency-domain analysis shows that by changing the scheme of the biaxial rotation mechanism, the initial alignment time is shortened and the accuracy of MEMS initial alignment is improved. At the same time, it is shown that the mean values are improved. A brief description is given of a parameter adjustment approach that allows the application of the proposed method to the self-alignment of different types of MEMS. The validity of this approach is verified by application to more than one type of MEMS.

The remainder of the paper is organized as follows. Section II defines the coordinate frames used in the paper. Section III is devoted to the scheme of biaxial rotation modulation and the error suppression principle of biaxial rotation modulation. Section IV presents a detailed description of the procedure of the MEMS strapdown compass initial self-alignment method. Section V presents a frequency-domain analysis of the scheme of biaxial rotation modulation, together with an experimental conformation of the analytical results. Section VI presents the parameter adjustment approach, based on an analysis of MEMS gyroscope noise in terms of the Allan variance. Using this approach, the proposed method can be applied to different types of MEMS, and this is verified experimentally. Finally, Section VII presents the conclusions of this paper.

II. COORDINATE FRAME DEFINITION

The coordinate frames used in the paper are defined as follows:

i frame: Earth-Centered Initially Fixed orthogonal reference frame. The x_i axis is in the equatorial plane and points to the vernal equinox, the z_i axis points to the earth's rotational direction, and the third axis constitutes the right hand coordinate system.

e frame: Earth-Centered Earth Fixed orthogonal reference frame. The x_e axis points to the central meridian in the equatorial plane, the z_e axis points to the earth's rotational direction, and the third axis constitutes the right hand coordinate system.

b frame: Carrier coordinate frame. It changes with the movement of carrier. Taking the ship as an example, the x_b axis points to the starboard of the ship, the y_b axis points to the bow of the ship, and the third axis constitutes the right hand coordinate system, pointing perpendicularly to the ship's deck plane.

n frame: Navigation coordinate frame. The orthogonal reference frame is aligned with the East-North-Up geodetic axes.

r frame: Rotating coordinate frame. The orthogonal reference frame is defined for the rotation modulation system, which rotates with the rotation mechanism. The rotating coordinate frame coincides with the carrier coordinate system before the rotation mechanism rotates. Three axes points to the sensitive axis directions of the IMU.

The coordinate frames are illustrated in Fig. 1, with the *i* frame and *e* frame at the top, the *b* frame and *n* frame in the middle, and the *r* frame at the bottom.

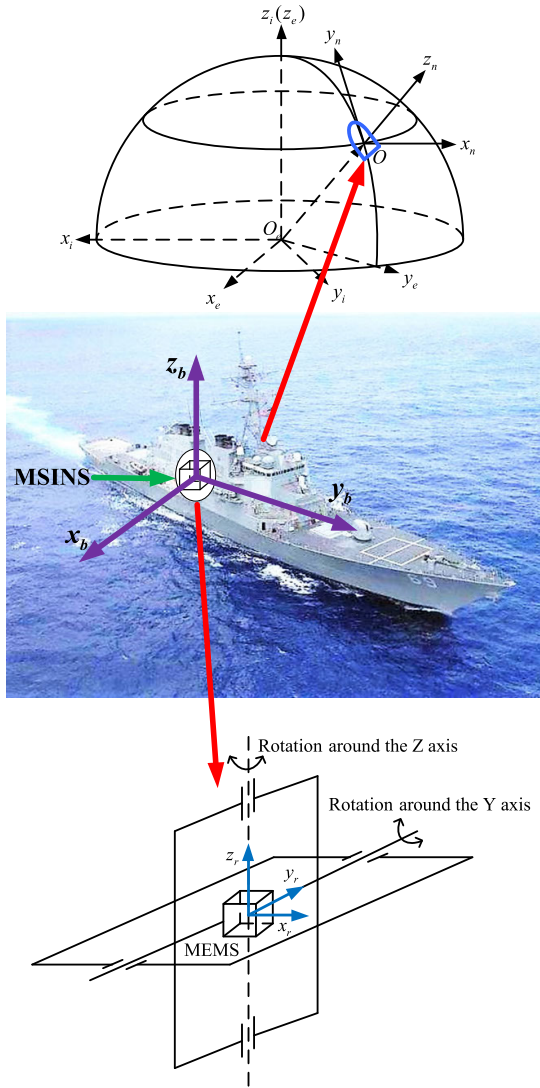


FIGURE 1. Definition of the coordinate frames.

III. BIAxIAL ROTATION MODULATION TECHNIQUE

A. BIAxIAL ROTATION MODULATION SCHEME

A biaxial rotation modulation scheme is adopted in this paper. In contrast to single-axis rotation modulation, biaxial rotation modulation is able to modulate the IMU drift of three axes. Biaxial rotation modulation obviously has a simpler structure than three-axis rotation modulation, thus helping to meet the requirement for a low-cost MSINS. The installation model diagram of the proposed MSINS biaxial rotation modulation scheme is shown in Fig. 2.

The MEMS biaxial rotation modulation scheme adopted in this paper is a 16-order intermittent stopping scheme, rotating around the z_b and y_b axes. Compared with other-order intermittent stopping schemes [15], the more complete error modulation characteristics are reflected by the 16-order intermittent stopping scheme. The procedure of 16-order biaxial rotation modulation is shown in Fig. 3. Taking the first four orders as an example, it can be described as follows. In the initial position A, the r frame of the MEMS coincides with

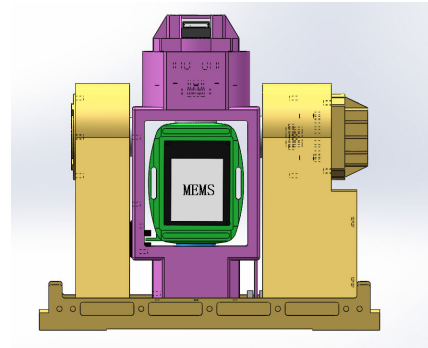


FIGURE 2. Model diagram of biaxial rotation modulation MSINS.

the b frame. At order 1, the MEMS positively rotates 180° around the z_b axis from position A to position B. At order 2, the MEMS positively rotates 180° around the y_b axis from position B to position C. At order 3, the MEMS negatively rotates 180° around the z_b axis from position C to position D. At order 4, the MEMS negatively rotates 180° around the y_b axis from position D to position A.

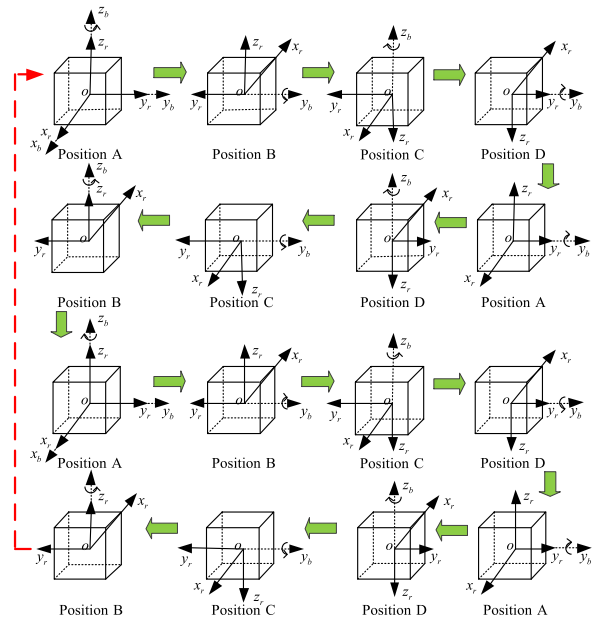


FIGURE 3. Process diagram of biaxial rotation modulation.

B. THEORY OF BIAxIAL ROTATION MODULATION

The biaxial rotation modulation scheme determines a rotation matrix C_r^b [16]. The navigational computation based on MEMS biaxial rotation modulation can be described as follows:

$$\begin{cases} \omega_{ir}^b = C_r^b \cdot \omega_{ir}^r \\ \omega_{rb}^b = -C_r^b \cdot \omega_{br}^r \\ \omega_{ib}^b = \omega_{ir}^b + \omega_{rb}^b \\ f^b = C_r^b f^r \end{cases} \quad (1)$$

where ω_{ir}^r is the output of the MEMS gyroscope in the r frame, ω_{br}^r is the angular velocity of the biaxial rotation

mechanism, and \mathbf{f}^r is the output of the MEMS accelerometer in the r frame.

The error modulation mechanisms, error propagation characteristics, and the design of the rotating scheme are analyzed in [16]. In the present paper, the error modulation characteristics of each state are analyzed separately, in particular with regard to the influence of MEMS gyroscope drift.

In a biaxial rotation modulation period, the constant gyroscope drift after integration can be expressed as follows:

$$\left\{ \begin{aligned} &4 \left(\int_0^{T_s} \varepsilon_x^b dt \right)_A + 4 \left(\int_0^{T_s} \varepsilon_x^b dt \right)_B + 4 \left(\int_0^{T_s} \varepsilon_x^b dt \right)_C \\ &\quad + 4 \left(\int_0^{T_s} \varepsilon_x^b dt \right)_D = 0 \\ &4 \left(\int_0^{T_s} \varepsilon_y^b dt \right)_A + 4 \left(\int_0^{T_s} \varepsilon_y^b dt \right)_B + 4 \left(\int_0^{T_s} \varepsilon_y^b dt \right)_C \\ &\quad + 4 \left(\int_0^{T_s} \varepsilon_y^b dt \right)_D = 0 \\ &4 \left(\int_0^{T_s} \varepsilon_z^b dt \right)_A + 4 \left(\int_0^{T_s} \varepsilon_z^b dt \right)_B + 4 \left(\int_0^{T_s} \varepsilon_z^b dt \right)_C \\ &\quad + 4 \left(\int_0^{T_s} \varepsilon_z^b dt \right)_D = 0 \end{aligned} \right. \quad (2)$$

where A, B, C, and D are the stopping positions in a biaxial rotation modulation period (see Fig. 3), ε is the constant MEMS gyroscope drift, and T_s is the stopping time after each rotation process.

According to (2), the result of modulation of the constant gyroscope drift is zero in the n frame during the stopping process.

In process 1 (orders 1, 3, 6, and 8), the constant gyroscope drifts along the x and y axes in the r frame are modulated by the changing regulation of the positive and negative periods. In the rotation orders of process 1, the constant gyroscope drift along the x axis after integration can be expressed as follows:

$$\left\{ \begin{aligned} &\left(\int_0^{T_z} \varepsilon_x^b dt \right)_{A \rightarrow B(+)} = \int_{0^\circ}^{180^\circ} (\varepsilon_x^r \cos \omega t + \varepsilon_y^r \sin \omega t) dt \\ &\quad = \frac{2}{\omega} \varepsilon_y^r \\ &\left(\int_0^{T_z} \varepsilon_x^b dt \right)_{B \rightarrow A(+)} = \int_{180^\circ}^{360^\circ} (\varepsilon_x^r \cos \omega t + \varepsilon_y^r \sin \omega t) dt \\ &\quad = -\frac{2}{\omega} \varepsilon_y^r \\ &\left(\int_0^{T_z} \varepsilon_x^b dt \right)_{C \rightarrow D(-)} = \int_{180^\circ}^{0^\circ} (\varepsilon_x^r \cos \omega t - \varepsilon_y^r \sin \omega t) dt \\ &\quad = \frac{2}{\omega} \varepsilon_y^r \\ &\left(\int_0^{T_z} \varepsilon_x^b dt \right)_{D \rightarrow C(-)} = \int_{360^\circ}^{180^\circ} (\varepsilon_x^r \cos \omega t - \varepsilon_y^r \sin \omega t) dt \\ &\quad = -\frac{2}{\omega} \varepsilon_y^r \end{aligned} \right. \quad (3)$$

where ω is the angular velocity of the biaxial rotation mechanism, and T_z is the rotation time of each rotation process.

Similarly, the results for the constant gyroscope drift along the y axis after integration can be expressed as follows:

$$\left\{ \begin{aligned} &\left(\int_0^{T_z} \varepsilon_y^b dt \right)_{A \rightarrow B(+)} = \int_{0^\circ}^{180^\circ} (-\varepsilon_x^r \sin \omega t + \varepsilon_y^r \cos \omega t) dt \\ &\quad = -\frac{2}{\omega} \varepsilon_x^r \\ &\left(\int_0^{T_z} \varepsilon_y^b dt \right)_{B \rightarrow A(+)} = \int_{180^\circ}^{360^\circ} (-\varepsilon_x^r \sin \omega t + \varepsilon_y^r \cos \omega t) dt \\ &\quad = \frac{2}{\omega} \varepsilon_x^r \\ &\left(\int_0^{T_z} \varepsilon_y^b dt \right)_{C \rightarrow D(-)} = \int_{180^\circ}^{0^\circ} (\varepsilon_x^r \sin \omega t + \varepsilon_y^r \cos \omega t) dt \\ &\quad = -\frac{2}{\omega} \varepsilon_x^r \\ &\left(\int_0^{T_z} \varepsilon_y^b dt \right)_{D \rightarrow C(-)} = \int_{360^\circ}^{180^\circ} (\varepsilon_x^r \sin \omega t + \varepsilon_y^r \cos \omega t) dt \\ &\quad = \frac{2}{\omega} \varepsilon_x^r \end{aligned} \right. \quad (4)$$

According to (3) and (4), the constant gyroscope drift after integration over the whole cycle is zero, which can be expressed as follows:

$$\left\{ \begin{aligned} &\left(\int_0^{T_z} \varepsilon_x^b dt \right)_{A \rightarrow B(+)} + \left(\int_0^{T_z} \varepsilon_x^b dt \right)_{C \rightarrow D(-)} \\ &\quad + \left(\int_0^{T_z} \varepsilon_x^b dt \right)_{D \rightarrow C(-)} + \left(\int_0^{T_z} \varepsilon_x^b dt \right)_{B \rightarrow A(+)} = 0 \\ &\left(\int_0^{T_z} \varepsilon_y^b dt \right)_{A \rightarrow B(+)} + \left(\int_0^{T_z} \varepsilon_y^b dt \right)_{C \rightarrow D(-)} \\ &\quad + \left(\int_0^{T_z} \varepsilon_y^b dt \right)_{D \rightarrow C(-)} + \left(\int_0^{T_z} \varepsilon_y^b dt \right)_{B \rightarrow A(+)} = 0 \end{aligned} \right. \quad (5)$$

Similarly, in process 2 (orders 2, 4, 5, and 7), the constant gyroscope drift along the x and z axes after integration over the whole cycle is zero, which can be expressed as follows:

$$\left\{ \begin{aligned} &\left(\int_0^{T_z} \varepsilon_x^b dt \right)_{B \rightarrow C(+)} + \left(\int_0^{T_z} \varepsilon_x^b dt \right)_{D \rightarrow A(-)} \\ &\quad + \left(\int_0^{T_z} \varepsilon_x^b dt \right)_{A \rightarrow D(-)} + \left(\int_0^{T_z} \varepsilon_x^b dt \right)_{C \rightarrow B(+)} = 0 \\ &\left(\int_0^{T_z} \varepsilon_z^b dt \right)_{B \rightarrow C(+)} + \left(\int_0^{T_z} \varepsilon_z^b dt \right)_{D \rightarrow A(-)} \\ &\quad + \left(\int_0^{T_z} \varepsilon_z^b dt \right)_{A \rightarrow D(-)} + \left(\int_0^{T_z} \varepsilon_z^b dt \right)_{C \rightarrow B(+)} = 0 \end{aligned} \right. \quad (6)$$

Process 3 (orders 9, 11, 14, and 16) is similar to process 1, and process 4 (orders 10, 12, 13 and 15) is similar to process 2. The constant gyroscope drift after integration over the whole cycle is zero.

According to the above analysis, the constant gyroscope drift is fully modulated over the whole period of rotation modulation. A similar conclusion can be drawn from the accelerometer analysis.

To sum up, the 16-order biaxial rotation modulation scheme achieves the requirement of modulating the three-axis errors of the IMU, inhibits the constant drift of the MEMS, and provides a suitable environment for the subsequent strapdown compass initial alignment.

IV. ROTATION MODULATION STRAPDOWN COMPASS INITIAL ALIGNMENT

A. THEORY OF ROTATION MODULATION STRAPDOWN COMPASS INITIAL ALIGNMENT

In the environment of biaxial rotation modulation [17], the initial alignment method of a MSINS is based on classical feedback control theory and the compass effect [18], which can be considered as the addition of a higher order low-pass filter based on the MSINS. Thus, noise in the MEMS is further inhibited, allowing the MEMS to be sensitive to the angular velocity of the earth and completing the self-alignment of the MSINS.

The schematic diagram and the control schematic diagram of the strapdown compass initial alignment with the eastward channel are shown in Fig. 4, respectively.

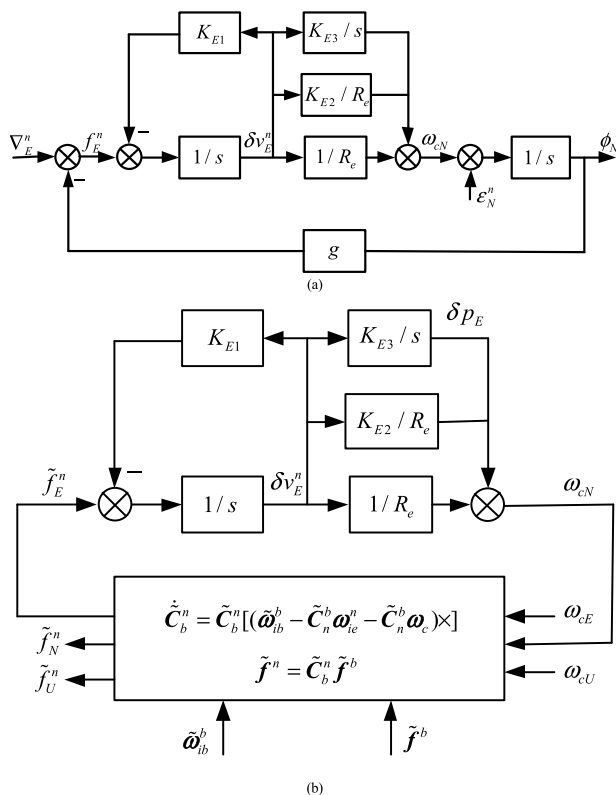


FIGURE 4. (a) Schematic diagram of the strapdown compass initial alignment with the eastward channel. (b) Control schematic diagram of the strapdown compass initial alignment with the eastward channel.

As shown in Fig. 4, s is the complex variable in the complex frequency domain, R_e is the radius of the earth, g is the acceleration due to gravity, K is the undetermined coefficient of the strapdown compass initial alignment, ω_c is the angular control rate, and δv is the intermediate variable.

According to Fig. 4(a), when the system input is the eastward accelerometer bias ∇_E , the eastward accelerometer bias ∇_E and the northward horizontal error angle ϕ_N are related as follows:

$$\phi_N(s) = \frac{(1 + K_{E2})s + K_{E3}R_e}{R_e s^3 + K_{E1}R_e s^2 + g(1 + K_{E2})s + gK_{E3}R_e} \cdot \nabla_E(s) \tag{7}$$

According to Fig. 4(a), when the system input is the northward gyroscope drift ε_N , the northward gyroscope drift ε_N and the northward horizontal error angle ϕ_N are related as follows:

$$\phi_N(s) = \frac{R_e s^2 + K_{E1}R_e s}{R_e s^3 + K_{E1}R_e s^2 + g(1 + K_{E2})s + gK_{E3}R_e} \cdot \varepsilon_N(s) \tag{8}$$

According to Fig. 4(b), the control equations for the eastward channel of the strapdown compass initial alignment can be discretized in the following form:

$$\begin{cases} \delta v_{Ek}^n = \delta v_{Ek-1}^n + (\tilde{f}_{Ek}^n - K_{E1}\delta v_{Ek-1}^n)T_0 \\ \delta p_{Ek} = \delta p_{Ek-1} + K_{E3}\delta v_{Ek}^n T_0 \\ \omega_{cNk} = \delta v_{Ek}^n(1 + K_{E2})/R_e + \delta p_{Ek} \end{cases} \tag{9}$$

where T_0 and $k(k = 1, 2, 3 \dots)$ are the update time and update frequency of the strapdown mathematics platform, respectively.

The schematic diagram and the control schematic diagram of the strapdown compass initial alignment with the northward channel are shown in Fig. 5, respectively.

According to Fig. 5(a), when the system input is the northward accelerometer bias ∇_N , the northward accelerometer bias ∇_N and the eastward horizontal error angle ϕ_E are related as follows:

$$\phi_E(s) = -\frac{(1 + K_{N2})s + K_{N3}R_e}{R_e s^3 + K_{N1}R_e s^2 + g(1 + K_{N2})s + gK_{N3}R_e} \cdot \nabla_N(s) \tag{10}$$

According to Fig. 5(a), when the system input is the eastward gyroscope drift ε_E , the eastward gyroscope drift ε_E and the eastward horizontal error angle ϕ_E are related as follows:

$$\phi_E(s) = -\frac{R_e s^2 + K_{N1}R_e s}{R_e s^3 + K_{N1}R_e s^2 + g(1 + K_{N2})s + gK_{N3}R_e} \cdot \varepsilon_E(s) \tag{11}$$

According to Fig. 5(a), when the system input is the azimuth error angle ϕ_U , the azimuth error angle ϕ_U and the eastward horizontal error angle ϕ_E are related as follows:

$$\phi_E(s) = -\frac{\omega_N R_e s^2 + K_{N1}\omega_N R_e s}{R_e s^3 + K_{N1}R_e s^2 + g(1 + K_{N2})s + gK_{N3}R_e} \cdot \phi_U(s) \tag{12}$$

According to Fig. 5(b), the control equations for the northward channel of the strapdown compass initial

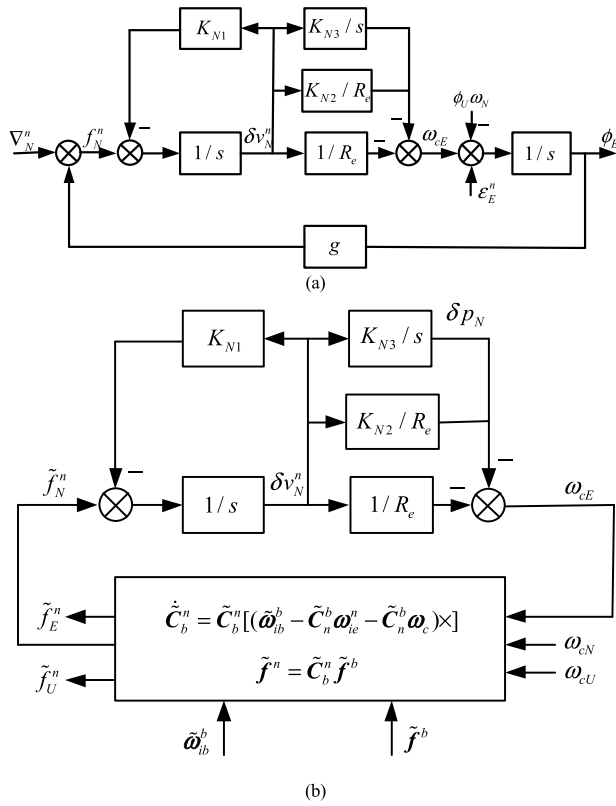


FIGURE 5. (a) Schematic diagram of the strapdown compass initial alignment with the northward channel. (b) Control schematic diagram of the strapdown compass initial alignment with the northward channel.

alignment can be discretized in the following form:

$$\begin{cases} \delta v_{Nk}^n = \delta v_{Nk-1}^n + (\tilde{f}_{Nk}^n - K_{N1} \delta v_{Nk-1}^n) T_0 \\ \delta p_{Nk} = \delta p_{Nk-1} + K_{N3} \delta v_{Nk}^n T_0 \\ \omega_{eEk} = -\delta v_{Nk}^n (1 + K_{N2}) / R_e - \delta p_{Nk} \end{cases} \quad (13)$$

The schematic diagram and the control schematic diagram of the strapdown compass initial alignment with the azimuth channel are shown in Fig. 6, respectively.

According to Fig. 6(a), when the system input is the northward accelerometer bias ∇_N , the northward accelerometer bias ∇_N and the azimuth error angle ϕ_U are related as follows:

$$\begin{aligned} \phi_U(s) &= -(K_{U3} R_e s) / \{\omega_N R_e s^4 + \omega_N R_e (K_{U1} + K_{U4}) s^3 \\ &\quad + \omega_N [R_e K_{U1} K_{U4} + g(1 + K_{U2})] s^2 + \omega_N g(1 + K_{U2}) K_{U4} s \\ &\quad + \omega_N R_e K_{U3} g\} \cdot \nabla_N(s) \end{aligned} \quad (14)$$

According to Fig. 6(a), when the system input is the up gyroscope drift ε_U , the up gyroscope drift ε_U and the azimuth error angle ϕ_U are related as follows:

$$\begin{aligned} \phi_U(s) &= (R_e g K_{U3}) / \{\omega_N R_e s^4 + \omega_N R_e (K_{U1} + K_{U4}) s^3 \\ &\quad + \omega_N [R_e K_{U1} K_{U4} + g(1 + K_{U2})] s^2 + \omega_N g(1 + K_{U2}) K_{U4} s \\ &\quad + \omega_N R_e K_{U3} g\} \cdot \varepsilon_U(s) \end{aligned} \quad (15)$$

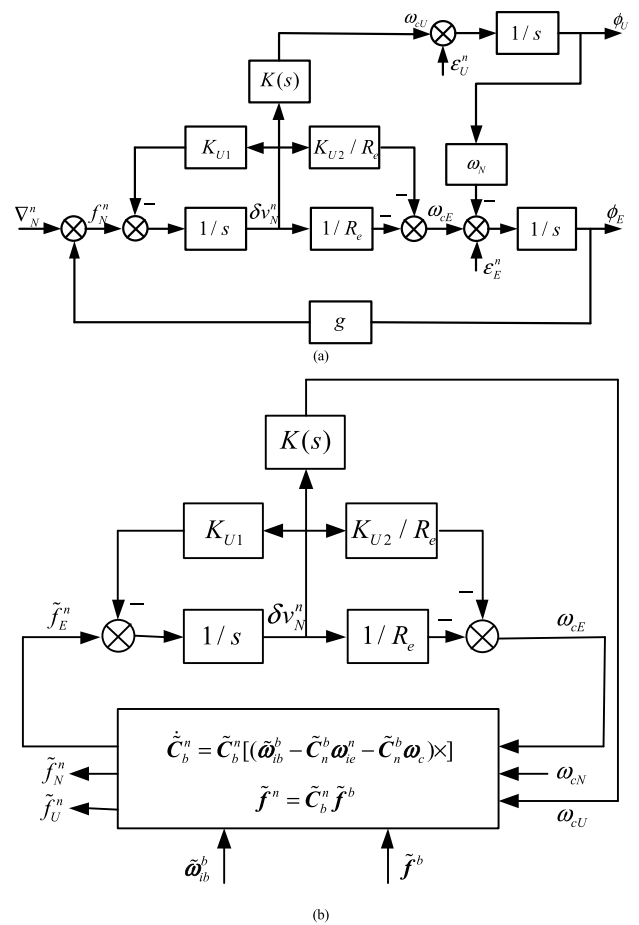


FIGURE 6. (a) Schematic diagram of the strapdown compass initial alignment with the azimuth channel. (b) Control schematic diagram of the strapdown compass initial alignment with the azimuth channel.

According to Fig. 6(a), when the system input is the eastward gyroscope drift ε_E , the eastward gyroscope drift ε_E and the azimuth error angle ϕ_U are related as follows:

$$\begin{aligned} \phi_U(s) &= \{R_e s^3 + R_e (K_{U1} + K_{U4}) s^2 + [R_e K_{U1} K_{U4} + g(1 + K_{U2})] s \\ &\quad + g(1 + K_{U2}) K_{U4}\} / \{R_e s^4 + R_e (K_{U1} + K_{U4}) s^3 \\ &\quad + [R_e K_{U1} K_{U4} + g(1 + K_{U2})] s^2 + g(1 + K_{U2}) K_{U4} s \\ &\quad + g K_{U3} R_e\} \cdot \varepsilon_E(s) \end{aligned} \quad (16)$$

According to Fig. 6(b), the control equations for the azimuth channel of the strapdown compass initial alignment can be discretized in the following form:

$$\begin{cases} \delta v_{Nk}^n = \delta v_{Nk-1}^n + (\tilde{f}_{Nk}^n - K_{U1} \delta v_{Nk-1}^n) T_0 \\ \omega_{eEk} = -\delta v_{Nk}^n (1 + K_{U2}) / R_e \\ \omega_{eUk} = (K_{U3} \delta v_{Nk}^n T_0 / \omega_N + \omega_{eUk-1}) / (1 + K_{U4} T_0) \\ K(s) = \frac{K_{U3}}{(s + K_{U4}) \omega_N} \end{cases} \quad (17)$$

where $\omega_N = \omega_{ie} \cos L$, L is the local latitude.

Considering that the MEMS gyroscope drift is not sensitive to the angular velocity of the earth, the method for

self-alignment method of MSINS proposed in this paper is combined with the rotation modulation technique and the compass loop. The control regulation of the compass loop is unchanged, but the updating process of the strapdown compass mathematical platform is improved. The mathematical platforms of the rotation modulation strapdown compass before and after improvement are shown in Fig. 7.

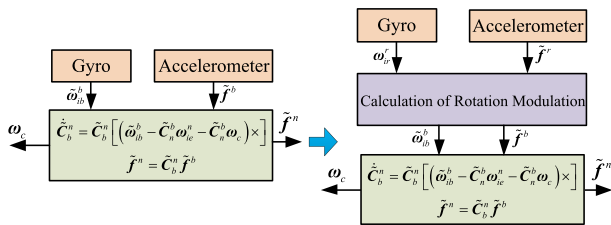


FIGURE 7. Mathematical platform of strapdown compass before and after improvement.

According to (a) in Fig. 4-Fig. 6, some signal flows represent the motion regulation of the platform and the other signal flows represent the control regulation of the initial alignment. According to (b) in Fig. 4-Fig. 6, the control regulation remains unchanged, but the mathematical platform is replaced by the improved version that takes account of the gyroscope and accelerometer measurement errors [19].

The initial alignment method for the MEMS strapdown compass can be summarized by the flowchart in Fig. 8.

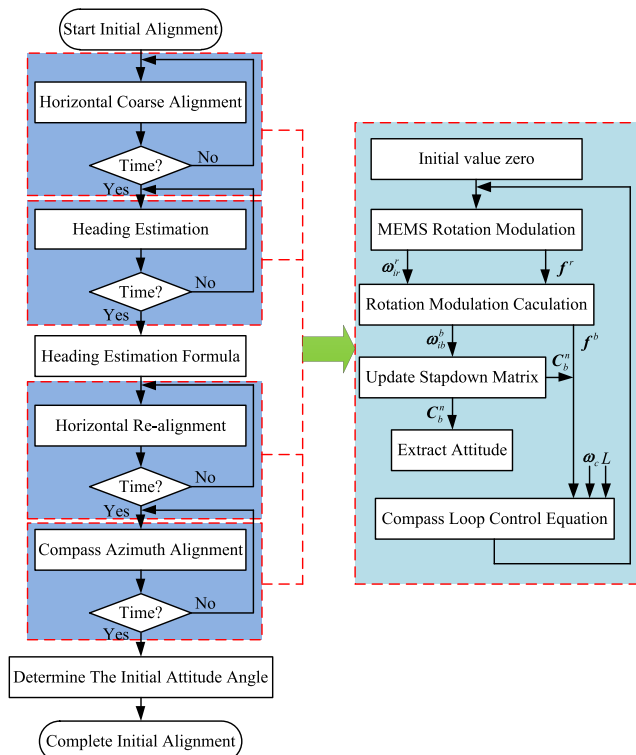


FIGURE 8. Initial alignment method flowchart for the MEMS strapdown compass.

As shown in Fig. 8, the details of the procedure are as follows:

Step1 (environment of MEMS initial self-alignment): The MEMS strapdown compass initial alignment is combined with the biaxial rotation modulation technique and the compass loop. The initial alignment is divided into two phases: coarse alignment and fine alignment. The coarse alignment process involves two steps: horizontal coarse alignment and heading estimation. The fine alignment process also involves two steps: horizontal re-alignment and compass azimuth alignment.

Step2 (horizontal coarse alignment): Select a time for horizontal coarse alignment. Since the initial attitude angles are unknown, the initial attitude angles are set to zero and the strapdown matrix is initialized to the identity matrix. Horizontal alignment is then achieved through the strapdown compass horizontal alignment channel.

Step3 (heading estimation): The derivative of the attitude error angle is expressed as:

$$\dot{\phi} = \omega^{\hat{n}} - C_n^{\hat{n}} \omega^n \tag{18}$$

and, since $\omega^{\hat{n}} = \omega^n + \omega^c$, this becomes:

$$\dot{\phi} = (I - C_n^{\hat{n}}) \omega^n + \omega^c \tag{19}$$

After step2, the horizontal attitude angle is known and can be regarded as a small error angle. Then, the derivative of the horizontal error angle is zero, and so its second-order terms can be ignored. Equation (19) can be simplified as:

$$\begin{cases} \omega_y^n \sin \phi_z - \omega_{cx} = 0 \\ \omega_y^n (1 - \cos \phi_z) + \omega_{cz} = 0 \end{cases} \tag{20}$$

According to (20), the heading estimate can be expressed as:

$$\phi_z = \arctan \frac{\omega_{cx}}{\omega_y^n + \omega_{cy}} \tag{21}$$

In practice, ω_{cx} is replaced by $\bar{\omega}_{cx}$. The error can be reduced by integrating ω_{cx} and then calculating the mean value of ω_{cx} . This can be expressed as:

$$\begin{cases} \bar{\omega}_{cx} = \frac{1}{T_{heading}} \int_0^{T_{heading}} \omega_{cx} dt \\ \bar{\omega}_{cy} = \frac{1}{T_{heading}} \int_0^{T_{heading}} \omega_{cy} dt \end{cases} \tag{22}$$

where $T_{heading}$ represents the time of the heading estimation.

Step4 (horizontal re-alignment): Select a time for horizontal re-alignment. After step3, the horizontal error angle in the mathematical platform may become larger, and therefore it needs horizontal realignment. Step4 is carried out under the conditions of a small heading error angle and lays the foundation for step5.

Step5 (compass azimuth alignment): Select a time for compass azimuth alignment. Horizontal alignment and compass azimuth alignment are carried out at the same time through the strapdown compass azimuth alignment channel.

Under conditions ensuring accuracy of horizontal alignment, the compass azimuth alignment is completed, which achieves the goal of azimuth alignment.

B. PARAMETER SELECTION

In this subsection, with reference to the traditional design method for compass alignment parameters [20], parameters appropriate for MEMS self-alignment are designed. The eastward alignment channel is taken as an example. For the strapdown compass designed in this paper, the horizontal alignment channel adjustment parameters can be expressed as:

$$\begin{cases} K_{E1} = 3\sigma_{level} \\ K_{E2} = \frac{\sigma_{level}^2(2 + 1/\xi_{level}^2)}{\omega_s^2} - 1 \\ K_{E3} = \frac{\sigma_{level}^3}{g\xi_{level}^2} \end{cases} \quad (23)$$

And the azimuth alignment channel adjustment parameters can be expressed as:

$$\begin{cases} K_{U1} = K_{U4} = 2\sigma_{heading} \\ K_{U2} = \frac{4\sigma_{heading}^2}{\omega_s^2} - 1 \\ K_{U3} = \frac{4\sigma_{heading}^4}{g} \end{cases} \quad (24)$$

where $\sigma = \omega_d \xi / \sqrt{1 - \xi^2}$ is the attenuation coefficient, $\omega_d = 2\pi/T_d$ is the damping oscillation frequency, ξ is the damping ratio, T_d is the damping oscillation period, and $\omega_s = \sqrt{g/R_e}$ is the 84.4 min Schuler frequency. The above parameters are all set equal to constants.

According to classical feedback control theory and the precision requirement for MEMS initial alignment, the parameters set in this subsection are:

$$\begin{cases} \xi_{level} = 0.707 \\ \xi_{heading} = 0.707 \\ T_{d_level} = 100s \\ T_{d_heading} = 400s \end{cases} \quad (25)$$

Substituting (25) into (23) and (24), the adjustment parameters for the horizontal and azimuth alignment channels are:

$$\begin{cases} K_{E1} = 1.885 \times 10^{-1}, & K_{E2} = 1.027 \times 10^4, & K_{E3} = 5.059 \times 10^{-5} \\ K_{U1} = 3.140 \times 10^{-2}, & K_{U2} = 6.409 \times 10^2 \\ K_{U3} = 2.483 \times 10^{-8}, & K_{U4} = 3.140 \times 10^{-2} \end{cases} \quad (26)$$

C. EXPERIMENTAL VALIDATION

Substituting (26) into (9), (13) and (17), the initial alignment method of MEMS biaxial rotation modulation strapdown compass is verified following the steps in Section IV A. The MEMS data are collected by MEMS ADIS16488A [21], whose main technical parameters are shown in Table 1.

TABLE 1. Main technical parameters of the MEMS ADIS16488A.

MEMS Gyroscopes	Minimum	Typical	Maximum	Unit
Dynamic range	±450		±480	°/s
Sensitivity		3.052×10 ⁻⁷		°/sec/LSB
Misalignment (axis to axis)		±0.05		°
Misalignment (axis to frame)		±1.0		°
Nonlinearity		0.01		% of FS
Bias repeatability		±0.2		°/s
In-run bias stability		5.1		°/h
Angular random walk		0.26		°/h
Output noise (without filtering)		0.135		°/s

The biaxial rotation modulation is performed by a low-precision biaxial rotation mechanism. The reference for the initial attitude angle and the simulation of the swinging base [22] are provided by a high-precision SGT-8 three-axis turntable, whose main technical parameters are shown in Table 2.

TABLE 2. Main technical parameters of the SGT-8 three-axis turntable.

	Inner Axis	Middle Axis	Outer Axis
Location accuracy of angular position	±2 arc sec	±2 arc sec	±3 arc sec
Maximum angular rate	±400 °/s	±250 °/s	±180 °/s
Rotation rate resolution	0.001 °/s	0.001 °/s	0.001 °/s

Before the experiments, the MEMS gyroscopes and accelerometers are calibrated in the traditional manner to avoid non-orthogonal errors [23]. The installation of the MEMS biaxial rotation mechanism on the SGT-8 three-axis turntable is shown in Fig. 9.

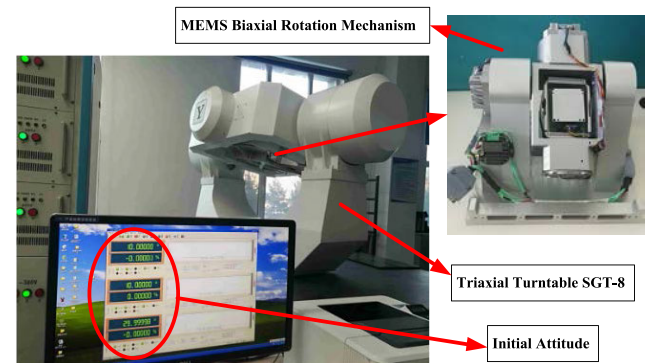


FIGURE 9. Installation diagram of MEMS biaxial rotation modulation strapdown inertial navigation system on three-axis turntable.

The experimental conditions for the biaxial rotation modulation of the MSINS on the SGT-8 three-axis turntable are shown in Table 3.

The initial alignment conditions of the MEMS biaxial rotation modulation strapdown compass on a swinging base are shown in Table 4.

TABLE 3. Experimental conditions for the biaxial rotation modulation of the MSINS on the SGT-8.

Experimental conditions	Numeric values
Initial latitude (°N)	45.7796
Initial longitude (°E)	126.6705
Initial attitude (°)	10, 10, 30
Swinging amplitude (°)	5, 5, 5
Swinging cycle (s)	10, 10, 10

TABLE 4. Initial alignment conditions for the MEMS biaxial rotation modulation strapdown compass.

Experimental conditions	Numeric values	Unit
Initial alignment time	50	min
Horizontal coarse alignment time	10	min
Heading estimation time	10	min
Horizontal re-alignment time	10	min
Compass azimuth alignment time	20	min
Angular velocity of biaxial rotation scheme	60	°/s
Rotation and stop times of biaxial rotation scheme	3 and 15	s

The experimental results for MSINS initial alignment are shown in Fig. 10, where the plots on the right are local magnifications of the sections from 30 or 40 min to 50 min.

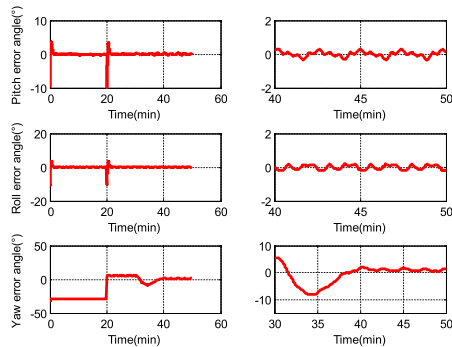


FIGURE 10. Experimental results for the initial alignment of the MEMS biaxial rotation modulation strapdown compass.

As shown in Fig. 10, the pitch error angle is 0.1129° , the roll error angle is -0.197° , and the yaw error angle is 1.474° . The yaw error angle converges perfectly at 50 min. These initial alignment results satisfy the initial alignment accuracy requirement for MSINS.

V. INITIAL ALIGNMENT BASED ON THE BIAxIAL ROTATION MECHANISM

A. STATEMENT OF THE PROBLEM

As shown by the results in Fig. 10, the proposed initial alignment method for a MEMS biaxial rotation modulation strapdown compass can provide the necessary precision of initial alignment. However, the initial alignment time is so long that this method is not sufficiently rapidly for practical application.

The initial alignment conditions for the MEMS biaxial rotation modulation strapdown compass on a swinging

base with the required shorter alignment times are shown in Table 5.

TABLE 5. Initial alignment conditions for the MEMS biaxial rotation modulation strapdown compass with shorter alignment times.

Experimental conditions	Numeric values	Unit
Initial alignment time	20	min
Horizontal coarse alignment time	5	min
Heading estimation time	5	min
Horizontal re-alignment time	5	min
Compass azimuth alignment time	5	min
Angular velocity of biaxial rotation scheme	60	°/s
Rotation and stop times of biaxial rotation scheme	3 and 15	s

The experimental results for MSINS initial alignment with shorter alignment times are shown in Fig. 11.

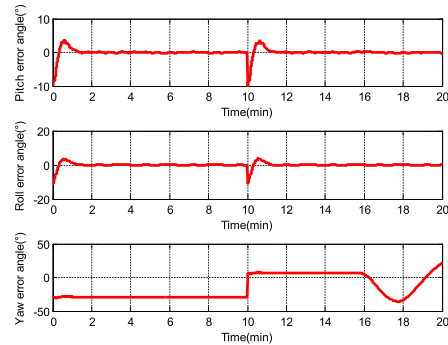


FIGURE 11. Experimental results for the initial alignment of the MEMS biaxial rotation modulation strapdown compass with shorter alignment times.

As can be seen from Fig. 11, the yaw error angle does not converge at 20 min. Thus, the approach of further shortening the initial alignment time is not feasible with the given experimental conditions. Therefore, the aim of the analysis in the following subsection is to find a way to effectively shorten the initial alignment time.

B. FREQUENCY-DOMAIN ANALYSIS OF INITIAL ALIGNMENT

The biaxial rotation modulation input angle frequency is one quarter of the rotation modulation period. In the previous biaxial rotation scheme, the rotation time was 3 s and the stop time was 15 s, while in the improved scheme, the rotation time becomes 2 s and the stop time becomes 10 s or 4 s. Meanwhile, the ship swinging cycle is set to 10 s. The input angle frequency for these different input conditions is as shown in Table 6.

TABLE 6. Input angle frequency of different input conditions.

Input conditions		Input angle frequency (rad/s)
Rotation time (s)	Stop time (s)	
3	15	0.0873
2	10	0.1309
2	4	0.2618
Swinging cycle (s)	10	0.6283

1) FREQUENCY-DOMAIN ANALYSIS OF NORTHWARD HORIZONTAL ERROR ANGLE

Substituting the parameters (26) into the control equations (7) and (8) gives the associated BODE diagrams shown in Fig. 12.

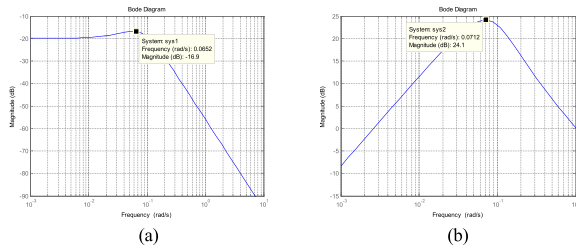


FIGURE 12. (a) Associated BODE diagram between the eastward accelerometer bias and the northward horizontal error angle. (b) Associated BODE diagram between the northward gyroscope drift and the northward horizontal error angle.

TABLE 7. Frequency-domain results for the northward error angle.

	ω_{Amax} (rad/s)	A_{max} (dB)	A_1 (dB)	A_2 (dB)	A_3 (dB)	A_4 (dB)
∇_E, ϕ_N	0.0652	-16.9	-17.5	-21.2	-34.3	-48.8
ϵ_N, ϕ_N	0.0712	24.1	23.7	20.5	13.5	3.81

According to Fig. 12, the corresponding frequency-domain results for the northward error angle are shown in Table 7.

Where ω_{Amax} is the input frequency when the system output amplitude is greatest, A_{max} is this maximum output amplitude, A_1 is the system output amplitude when the system input frequency is $0.0873rad/s$, A_2 is the system output amplitude when the system input frequency is $0.1309rad/s$, A_3 is the system output amplitude when the system input frequency is $0.2618rad/s$, and A_4 is the system output amplitude when the system input frequency is $0.6283rad/s$. The same notation is also used in Table 8 and 9.

TABLE 8. Frequency-domain results for the eastward error angle.

	ω_{Amax} (rad/s)	A_{max} (dB)	A_1 (dB)	A_2 (dB)	A_3 (dB)	A_4 (dB)
∇_N, ϕ_E	0.0652	-16.9	-17.5	-21.2	-34.3	-48.8
ϵ_E, ϕ_E	0.0712	24.1	23.7	20.5	13.5	3.81
ϕ_U, ϕ_E	0.0712	-61.8				

TABLE 9. Frequency-domain results for the azimuth error angle.

	ω_{Amax} (rad/s)	A_{max} (dB)	A_1 (dB)	A_2 (dB)	A_3 (dB)	A_4 (dB)
∇_N, ϕ_U	0.0183	28	-2.72	-12.9	-33.3	-53.6
ϵ_U, ϕ_U	0.0082	41.9	21.4	18.7	14.7	12.6
ϵ_E, ϕ_U	0.0124	85.1	38.3	24.7	-2.5	-29.6

As can be seen from Fig. 12 and Table 7, the influence of the eastward accelerometer bias and the northward gyroscope drift on the northward horizontal error angle has low-pass characteristics. When the input frequency is higher than ω_{Amax} , the system can suppress the resulting oscillating error in the northward horizontal error angle and produce a stable output.

It is found that the oscillation error can be suppressed by speeding up the rotation and reducing the stop-time of the biaxial rotation mechanism and that the influence of ship swinging on initial alignment can be reduced.

2) FREQUENCY-DOMAIN ANALYSIS OF EASTWARD HORIZONTAL ERROR ANGLE

Substituting the parameters (26) into the control equations (10), (11), and (12) gives the associated BODE diagrams shown in Fig. 13.

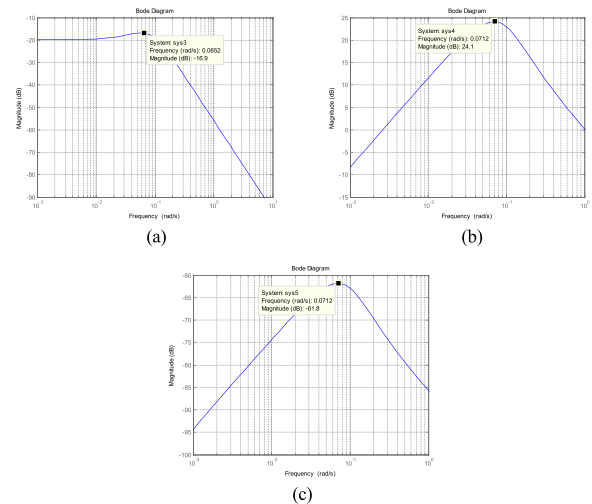


FIGURE 13. (a) Associated BODE diagram between the northward accelerometer bias and the eastward horizontal error angle. (b) Associated BODE diagram between the eastward gyroscope drift and the eastward horizontal error angle. (c) Associated BODE diagram between the azimuth error angle and the eastward horizontal error angle.

According to Fig. 13, the corresponding frequency-domain results for the eastward error angle are shown in Table 8.

As can be seen from Fig. 13 and Table 8, the influence of the northward accelerometer bias, the eastward gyroscope drift, and the eastward horizontal error angle on the eastward horizontal error angle has low-pass characteristics. When the input frequency is higher than ω_{Amax} , the system can suppress the resulting oscillating error in the eastward horizontal error angle and produce a stable output.

It is again found that the oscillation error can be suppressed by speeding up the rotation and reducing the stop-time of the biaxial rotation mechanism and that the influence of ship swinging on initial alignment can be reduced.

3) FREQUENCY-DOMAIN ANALYSIS OF AZIMUTH ERROR ANGLE

Substituting the parameters (26) into the control equations (14), (15), and (16) gives the associated BODE diagrams shown in Fig. 14.

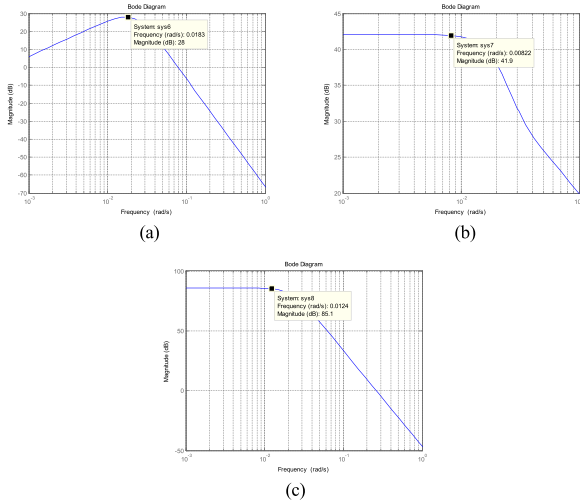


FIGURE 14. (a) Associated BODE diagram between the northward accelerometer bias and the azimuth error angle. (b) Associated BODE diagram between the azimuth gyroscope drift and the azimuth error angle. (c) Associated BODE diagram between the eastward gyroscope drift and the azimuth error angle.

According to Fig. 14, the corresponding frequency-domain results for the azimuth error angle are shown in Table 9.

As can be seen from Fig. 14 and Table 9, the influence of the northward accelerometer bias, the azimuth gyroscope drift, and the eastward gyroscope drift on the azimuth error angle has low-pass characteristics. When the input frequency is higher than $\omega_{A \max}$, the system can suppress the resulting oscillating error in the azimuth error angle and produce a stable output.

Yet again, it is found that the oscillation error can be suppressed by speeding up the rotation and reducing the stop-time of the biaxial rotation mechanism and that the influence of ship swinging on initial alignment can be reduced.

C. EXPERIMENTAL VALIDATION

1) SPEEDING UP THE ANGULAR VELOCITY OF THE BIAxIAL ROTATION MECHANISM

With the same experimental conditions as in Section IV C, the MEMS biaxial rotation modulation initial alignment is verified by speeding up the angular velocity of the biaxial rotation mechanism.

The initial alignment conditions of the MEMS biaxial rotation modulation strapdown compass on a swinging base with higher rotational angular velocity of the biaxial rotation mechanism are shown in Table 10.

The experimental results are shown in Fig. 15, where the plots on the right are local magnifications of the sections from 15 min to 20 min.

TABLE 10. Initial alignment conditions for the MEMS biaxial rotation modulation strapdown compass with higher angular velocity of biaxial rotation mechanism.

Experimental conditions	Numeric values	Unit
Initial alignment time	20	min
Horizontal coarse alignment time	5	min
Heading estimation time	5	min
Horizontal re-alignment time	5	min
Compass azimuth alignment time	5	min
Angular velocity of biaxial rotation scheme	90	°/s
Rotation and stop times of biaxial rotation scheme	2 and 10	s

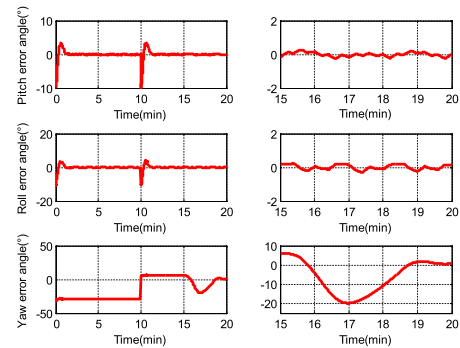


FIGURE 15. Experimental results for the initial alignment of the MEMS biaxial rotation modulation strapdown compass with higher rotational angular velocity of biaxial rotation mechanism.

It can be seen from Fig. 15 that the pitch error angle is -0.003° , the roll error angle is -0.158° , and the yaw error angle is 0.7922° . The yaw error angle converges perfectly at 20 min. These initial alignment results satisfy the initial alignment accuracy requirement for MSINS.

The initial alignment conditions for the MEMS biaxial rotation modulation strapdown compass on a swinging base with further shorter alignment times are shown in Table 11.

TABLE 11. Initial alignment conditions for the MEMS biaxial rotation modulation strapdown compass with further shorter alignment times.

Experimental conditions	Numeric values	Unit
Initial alignment time	15	min
Horizontal coarse alignment time	3	min
Heading estimation time	3	min
Horizontal re-alignment time	3	min
Compass azimuth alignment time	6	min
Angular velocity of biaxial rotation scheme	90	°/s
Rotation and stop times of biaxial rotation scheme	2 and 10	s

The experimental results with further shorter alignment times are shown in Fig. 16, where the plots on the right are local magnifications of the sections from 8 min to 15 min.

As can be seen from Fig. 16, the yaw error angle does not converge at 15 min. Thus, the approach of further shortening the initial alignment time is again not feasible with the given experimental conditions. To further shorten the initial alignment time, it is necessary to reduce the stop-time of the biaxial

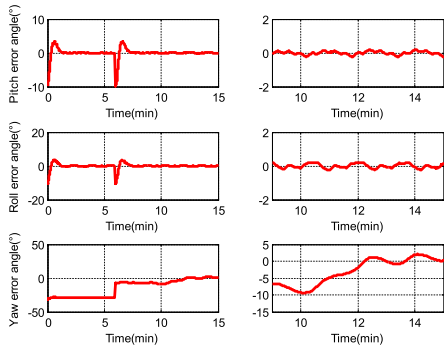


FIGURE 16. Experimental results for the initial alignment of the MEMS biaxial rotation modulation strapdown compass with higher rotational angular velocity of biaxial rotation mechanism and shorter alignment time.

rotation mechanism while speeding up the angular velocity of the biaxial rotation mechanism.

2) REDUCING THE STOP-TIME OF THE BIAxIAL ROTATION MECHANISM

The initial alignment conditions of the MEMS biaxial rotation modulation strapdown compass on a swinging base with reduced stop time and greater angular velocity of the biaxial rotation mechanism are shown in Table 12.

TABLE 12. Initial alignment conditions for the MEMS biaxial rotation modulation strapdown compass with shorter stop-time of the biaxial rotation mechanism.

Experimental conditions	Numeric values	Unit
Initial alignment time	15	min
Horizontal coarse alignment time	3	min
Heading estimation time	3	min
Horizontal re-alignment time	3	min
Compass azimuth alignment time	6	min
Angular velocity of biaxial rotation scheme	90	°/s
Rotation and stop times of biaxial rotation scheme	2 and 4	s

The experimental results are shown in Fig. 17, where the plots on the right are local magnifications of the sections from 8 min to 15 min.

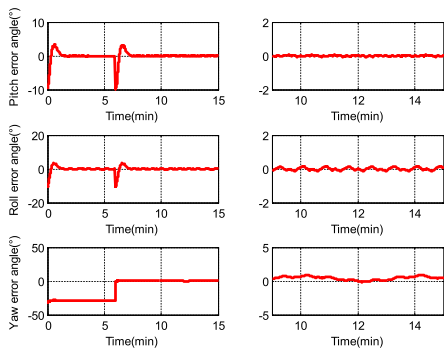


FIGURE 17. Experimental results for the initial alignment of the MEMS biaxial rotation modulation strapdown compass with shorter stop-time of biaxial rotation mechanism.

As can be seen from Fig. 17, the pitch error angle is 0.012° , the roll error angle is 0.062° , and the yaw error angle almost converges at 15 minutes. The initial alignment results satisfy the initial alignment accuracy requirement for MSINS.

VI. INITIAL ALIGNMENT BASED ON DIFFERENT TYPES OF MEMS

A. STATEMENT OF THE PROBLEM

The MEMS-IMU used in the above initial alignment experiments was an ADIS16488A. The question arises as to whether the method proposed in this paper is applicable for other types of MEMS. Therefore, an approach is proposed that allows the method to be used with different MEMS. In this approach, the initial alignment parameters of the MEMS rotation modulation strapdown compass are adjusted appropriately.

B. NOISE ANALYSIS OF MEMS GYROSCOPE

The MEMS-IMU ADIS16488A is installed on the SGT-8 three-axis turntable at room temperature on a static base. The sampling time is set to 2 h and the sampling frequency is set to 100 Hz. When the output of the MEMS is stable, an Allan variance analysis is performed on the data collected by the MEMS ADIS16488A gyroscope. The results [24] are shown in Fig. 18 and Table 13.

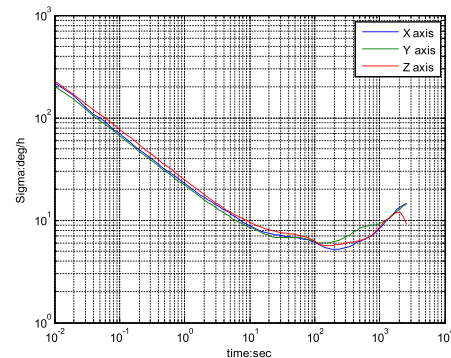


FIGURE 18. Allan variance of MEMS ADIS16488A.

TABLE 13. Allan variance calculation results of MEMS ADIS16488A.

Noise items	X-Axis	Y-Axis	Z-Axis	Unit
Quantization Noise	0.36	0.40	0.50	deg/h
Angular Random Walk	0.37	0.36	0.41	deg/h ^{0.5}
Bias Instability	10.11	2.63	7.68	deg/h
Rate Random Walk	44.15	37.00	25.75	deg/h/h ^{0.5}
Rate Ramp	30.53	23.42	15.48	deg/h/h

where the blue, green, and red lines represent the Allan variance on the x, y, and z axes, respectively.

These results can be taken as a standard on the basis of which the alignment parameters of the MEMS strapdown compass can be adjusted.

C. ADJUSTMENT OF INITIAL ALIGNMENT PARAMETERS OF MEMS ROTATION MODULATION STRAPDOWN COMPASS

The main difficulty with MEMS initial self-alignment lies in the compass azimuth alignment. Therefore the focus here is on adjustment of the azimuth alignment parameters, with only minor changes to the horizontal alignment parameters being considered.

The damping oscillation period T_d in (24) is chosen as the adjustment parameter for initial alignment. If a shorter alignment time is required, T_d should be set to a smaller value. However, interference from the environment and the limited precision of the MEMS usually mean that T_d cannot be chosen with too small a value.

As shown in Fig. 6(a), the limiting accuracy of ϕ_U in the azimuth alignment channel of the strapdown compass can be expressed as:

$$\phi_U(\infty) = \frac{\varepsilon_E}{\omega_N} + \frac{(K_{U2} + 1)K_{U4}}{R_e K_{U3}} \varepsilon_U \quad (27)$$

Substitution of (25) into (27) shows that the limiting accuracy of azimuth alignment can be simplified to:

$$\begin{aligned} \phi_U(\infty) &= \frac{\varepsilon_E}{\omega_N} + \frac{(4\sigma^2/\omega_s^2) \cdot (2\sigma)}{R_e \cdot 4\sigma^4/g} \varepsilon_U \\ &= \frac{\varepsilon_E}{\omega_N} + \frac{2}{\sigma} \varepsilon_U = \frac{\varepsilon_E}{\omega_N} + 2 \frac{T_d}{T_{ie}} \cos L \cdot \frac{\varepsilon_U}{\omega_N} \end{aligned} \quad (28)$$

The gyroscope drift in (28) is modulated by the biaxial rotation modulation as follows:

$$\begin{cases} \varepsilon_{E_after} = \varepsilon_{E_before} \sin\left(\frac{2\pi}{T_{round}}t\right) \\ \varepsilon_{U_after} = \varepsilon_{U_before} \sin\left(\frac{2\pi}{T_{round}}t\right) \end{cases} \quad (29)$$

where T_{round} is the rotation period of the biaxial rotation modulation.

Thus, the accuracy of MEMS azimuth alignment can be improved by reducing the rotational period of biaxial rotation modulation. Furthermore, the effect of the azimuth gyroscope drift on azimuth alignment accuracy can be reduced by selecting a smaller T_d . However, T_d must be large enough to prevent interference in the initial self-alignment method. An explicit relationship between the initial alignment of the rotation modulation strapdown compass and the MEMS gyroscope noise cannot be obtained owing to the complicated way in which these are connected. Therefore, the parameter T_d is adjusted on an empirical basis within a certain range.

The approach can be summarized as follows. First, the Allan variance and each noise item coefficient of a given MEMS gyroscope are calculated. These are then compared with the Allan variance and the noise item coefficients of the MEMS ADIS16488A gyroscope used in the present study. When the noise value of the given MEMS gyroscope is larger than that of the MEMS ADIS16488A gyroscope, the value of T_d is increased appropriately, although it should not exceed 2000 s, since an excessive value will lead to a

failure of convergence of the initial alignment results and make the initial alignment time too long. When the noise value of the given MEMS gyroscope is smaller than that of the MEMS ADIS16488A gyroscope, the value of T_d is decreased appropriately, but it should not be less than 60 s, since too low a value will lead to poor initial alignment accuracy. Thus, the parameter T_d can only be obtained by constant adjustment.

D. EXPERIMENTAL VALIDATION

To verify the correctness of the approach of adjusting the initial alignment parameters of the MEMS rotation modulation strapdown compass, a different type of MEMS-IMU, namely, the ADIS16460AMLZ, is selected.

The experimental conditions are the same as in Section VI B. The Allan variance and the noise item coefficients of the ADIS16460AMLZ gyroscope are shown in Fig. 19 and Table 14.

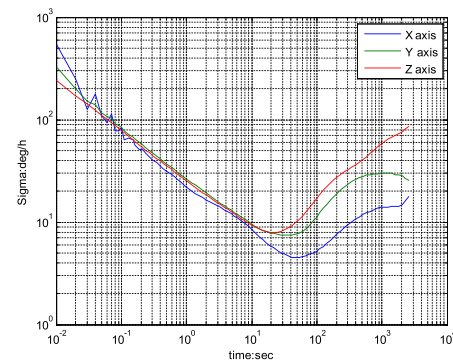


FIGURE 19. Allan variance results of MEMS ADIS16460AMLZ.

TABLE 14. Allan variance calculation results of MEMS ADIS16460AMLZ.

Noise items	X-Axis	Y-Axis	Z-Axis	Unit
Quantization Noise	3.18	1.23	0.23	deg/h
Angular Random Walk	0.16	0.41	0.41	deg/h ^{0.5}
Bias Instability	42.75	15.85	3.84	deg/h
Rate Random Walk	126.83	114.68	198.50	deg/h/h ^{0.5}
Rate Ramp	121.23	103.48	93.97	deg/h/h

where the blue, green, and red lines represent the Allan variance results on the x, y, and z axes, respectively.

From a comparison of Table 13 and 14, it can be seen that the noise item coefficients of MEMS ADIS16460AMLZ are larger than those of MEMS ADI16488A. According to the proposed approach, the azimuth damping oscillation period $T_{d_heading}$ is adjusted to 500 s, with the other parameters remaining.

Substitution of these parameters into (23) and (24) gives the parameters of the horizontal and azimuth alignment channel as:

$$\begin{cases} K_{E1} = 1.885 \times 10^{-1}, & K_{E2} = 1.027 \times 10^4, & K_{E3} = 5.059 \times 10^{-5} \\ K_{U1} = 2.510 \times 10^{-2}, & K_{U2} = 4.098 \times 10^2 \\ K_{U3} = 1.017 \times 10^{-8}, & K_{U4} = 2.510 \times 10^{-2} \end{cases} \quad (30)$$

On substitution of (30) into (9), (13) and (17), the initial alignment of the MEMS biaxial rotation modulation strapdown compass is verified following the steps in Section IV A. The MEMS data are collected by the MEMS-IMU ADIS16460AMLZ, whose main technical parameters are shown in Table 15.

TABLE 15. Main technical parameters of the MEMS ADIS16460AMLZ.

MEMS Gyroscopes	Minimum	Typical	Maximum	Unit
Dynamic range	±100		±480	°/s
Sensitivity		7.63×10^{-8}		°/sec/LSB
Misalignment (axis to axis)		±0.15		°
Misalignment (axis to frame)		±1.0		°
Nonlinearity		0.5		% of FS
Bias repeatability		0.5		°/s
In-run bias stability		8		°/h
Angular random walk		0.17		°/h
Output noise (without filtering)		0.075		°/s

The initial alignment conditions of the MEMS ADIS16460AMLZ biaxial rotation modulation strapdown compass on a swinging base are shown in Table 16. The purpose of extending the compass azimuth alignment time is to verify whether the yaw angle error converges.

TABLE 16. Initial alignment conditions for the MEMS ADIS16460AMLZ biaxial rotation modulation strapdown compass.

Experimental conditions	Numeric values	Unit
Initial alignment time	18	min
Horizontal coarse alignment time	3	min
Heading estimation time	3	min
Horizontal re-alignment time	3	min
Compass azimuth alignment time	9	min
Angular velocity of biaxial rotation scheme	90	°/s
Rotation and stop times of biaxial rotation scheme	2 and 4	s

The experimental results are shown in Fig. 20, where the plots on the right are local magnifications of the sections from 9 min to 18 min.

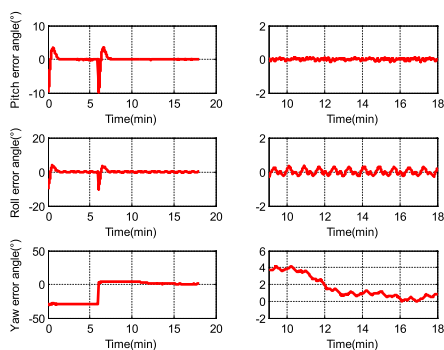


FIGURE 20. Experimental results for the initial alignment of the MEMS ADIS16460AMLZ biaxial rotation modulation strapdown compass.

As can be seen from Fig. 20, the pitch error angle is 0.003° , the roll error angle is 0.159° , and the yaw error angle is 1.176° . The yaw error angle almost converges at 15 min. The initial alignment results satisfy the initial alignment accuracy requirement for MSINS. The validity of the initial alignment parameter adjustment approach is thus confirmed.

VII. CONCLUSION

This paper has focused on the initial self-alignment of MSINS for marine applications. A novel method has been presented, applied to a rotating MEMS strapdown compass. First, based on an analysis of biaxial rotation modulation and initial alignment of the MEMS strapdown compass, a self-alignment method for the rotating MEMS strapdown compass has been presented and verified. Second, by analyzing the biaxial rotation modulation, the self-alignment of the MSINS has been improved by speeding up the rotation and reducing the stop time of the biaxial rotation mechanism to shorten the initial alignment time, which can effectively suppress the influence of MEMS noise on the initial alignment error angle. The influence of ship swinging on the initial alignment error angle has also been briefly analyzed. The efficiency of the method has been verified by experiments on a swinging base. Finally, a parameter adjustment approach has been presented that allows the proposed method to be used with different types of MEMS. This approach has been verified by experiments. All the experimental results demonstrate the efficiency of the proposed method and its suitability for practical application.

REFERENCES

- [1] S. Guo, J. Xu, and H. He, "External velocity aided coarse attitude and position alignment for dynamic SINS," *IEEE Access*, vol. 6, pp. 15099–15105, 2018.
- [2] D. Tomaszewski, J. Rapiński, and M. Śmieja, "Analysis of the noise parameters and attitude alignment accuracy of INS conducted with the use of MEMS-based integrated navigation system," *Acta Geodyn. Geomaterialia*, vol. 12, no. 2, pp. 197–208, May 2015.
- [3] W. Li and J. Wang, "Effective adaptive Kalman filter for MEMS-IMU/magnetometers integrated attitude and heading reference systems," *J. Navigat.*, vol. 66, no. 1, pp. 99–113, 2013.
- [4] P. Chen, "Attitude determination algorithms for spinning satellites using single antenna GPS receiver and MEMS gyro," *Aerosp. Sci. Technol.*, vol. 26, no. 1, pp. 10–15, Apr./May 2013.
- [5] Q. Xu, X. Li, and C.-Y. Chan, "Enhancing localization accuracy of MEMS-INS/GPS/in-vehicle sensors integration during GPS outages," *IEEE Trans. Instrum. Meas.*, vol. 67, no. 8, pp. 1966–1978, Aug. 2018.
- [6] H. Chu, T. Sun, B. Zhang, H. Zhang, and Y. Chen, "Rapid transfer alignment of MEMS SINS based on adaptive incremental Kalman filter," *Sensors*, vol. 17, no. 1, pp. 152–165, Jan. 2017.
- [7] F. O. Silva, E. M. Hemerly, and W. C. L. Filho, "Error analysis of analytical coarse alignment formulations for stationary SINS," *IEEE Trans. Aerosp. Electron. Syst.*, vol. 52, no. 4, pp. 1777–1796, Aug. 2016.
- [8] L. Zhao, D. Guan, J. Cheng, X. Xu, and Z. Fei, "Coarse alignment of marine strapdown INS based on the trajectory fitting of gravity movement in the inertial space," *Sensors*, vol. 16, no. 10, pp. 1714–1729, Oct. 2016.
- [9] H. Xing, Z. Chen, H. Yang, C. Wang, Z. Lin, and M. Guo, "Self-alignment MEMS IMU method based on the rotation modulation technique on a swing base," *Sensors*, vol. 18, no. 4, pp. 1178–1199, Apr. 2018.
- [10] Y. Jia, S. Li, Y. Qin, and R. Cheng, "Error analysis and compensation of MEMS rotation modulation inertial navigation system," *IEEE Sensors J.*, vol. 18, no. 5, pp. 2023–2030, Mar. 2018.
- [11] X. Wang, J. Wu, T. Xu, and W. Wang, "Analysis and verification of rotation modulation effects on inertial navigation system based on MEMS sensors," *J. Navigat.*, vol. 66, no. 5, pp. 751–772, 2013.

- [12] H. Hu, L. Zhang, H. Yan, Y. Bai, and P. Wang, "Denoising and baseline drift removal method of MEMS hydrophone signal based on VMD and wavelet threshold processing," *IEEE Access*, vol. 7, no. 1, pp. 59913–59922, May 2019.
- [13] X. Guo, C. Sun, P. Wang, and L. Huang, "A hybrid method for MEMS gyroscope signal error compensation," *Sensor Rev.*, vol. 38, no. 4, pp. 517–525, Sep. 2018.
- [14] D. Wang, H. Lv, and J. Wu, "In-flight initial alignment for small UAV MEMS-based navigation via adaptive unscented Kalman filtering approach," *Aerosp. Sci. Technol.*, vol. 61, pp. 73–84, Feb. 2017.
- [15] Z. Liu, L. Wang, K. Li, and J. Sui, "An improved rotation scheme for dual-axis rotational inertial navigation system," *IEEE Sensors J.*, vol. 17, no. 13, pp. 4189–4196, Jul. 2017.
- [16] Z. Jing, J. Li, X. Zhang, K. Feng, and T. Zheng, "A novel rotation scheme for MEMS IMU error mitigation based on a missile-borne rotation semi-strapdown inertial navigation system," *Sensors*, vol. 19, no. 7, pp. 1683–1704, Apr. 2019.
- [17] J. Zhang, J. Li, X. Che, X. Zhang, C. Hu, K. Feng, and T. Xu, "The optimal design of modulation angular rate for MEMS-based rotary semi-SINS," *Micromachines*, vol. 10, no. 2, pp. 111–123, Feb. 2019.
- [18] Y. Ben, Q. Zhang, X. Zang, L. Huang, Q. Li, and G. Wang, "Effect of the outer lever arm on in-motion gyrocompass alignment for fiber-optic gyro strapdown inertial navigation system," *Opt. Eng.*, vol. 56, no. 4, pp. 044106-1–044106-13, Apr. 2017.
- [19] G. Yan, "On SINS in-movement initial alignment and some other problems," Northwestern Polytech. Univ., Xi'an, China, Tech. Rep., Nov. 2008.
- [20] F. Li, J. Xu, and H. He, "Backtracking velocity denoising based autonomous in-motion initial alignment," *IEEE Access*, vol. 6, pp. 67144–67155, 2018.
- [21] H. Tian, Y. Liu, J. Zhou, Y. Wang, J. Wang, and W. Zhang, "Attitude angle compensation for a synchronous acquisition method based on an MEMS sensor," *Sensors*, vol. 19, no. 3, pp. 483–500, Jan. 2019.
- [22] Y. Liu, X. Xu, X. Liu, Y. Yao, L. Wu, and J. Sun, "A self-alignment algorithm for SINS based on gravitational apparent motion and sensor data denoising," *Sensors*, vol. 15, no. 5, pp. 9827–9853, Apr. 2015.
- [23] R. Fontanella, D. Accardo, R. S. L. Moriello, L. Angrisani, and D. De Simone, "MEMS gyros temperature calibration through artificial neural networks," *Sens. Actuators A, Phys.*, vol. 279, pp. 553–565, Aug. 2018.
- [24] J. Song, Z. Shi, L. Wang, and H. Wang, "Random error analysis of MEMS gyroscope based on an improved DAVAR algorithm," *Micromachines*, vol. 9, no. 8, pp. 373–394, Jul. 2018.



WEIQUAN HUANG received the B.S. degree in underwater acoustic electronics from the Harbin Shipbuilding Engineering Institute, in 1989, and the M.S. degree in information and signal processing and the Ph.D. degree in control theory and control engineering from Harbin Engineering University, in 1994 and 2006, respectively. He is currently a Professor with the College of Automation, Harbin Engineering University. His current research interests include underwater navigation, integrated navigation technology and new inertial devices, high-precision navigation systems, and MEMS inertial navigation systems.



MENGHAO LI received the B.S. degree from the College of Automation, Harbin Engineering University, Harbin, China, in 2016, where he is currently pursuing the Ph.D. degree in control science and engineering. His current research interests include MEMS inertial navigation systems, MEMS biaxial rotation modulation strapdown inertial navigation systems, information fusion, and its application in MEMS integrated navigation systems.

•••